LA-UR-18-31006
Approved for public release; distribution is unlimited.

Title: Applications of Analytic Models to Spent Fuel Cask Analysis

Author(s): Remedes, Tyler Joseph

Intended for: PhD Thesis Proposal

Issued: 2018-11-20

University of Florida

Doctorate of Philosophy Proposal Defense

Applications of Analytic Models to Spent Fuel Cask Analysis

Author:
Tyler J. Remedes
Comittee Chair:
Dr. James Baciak
Mentors:
Dr. Scott Ramsey
Mr. Joseph Schmidt
Comittee:
Dr. Andreas Enqvist
Dr. Justin Watson
Dr. Heather Ray

November 16, 2018

Abstract

The advent of high performance computing has changed the way scientists and engineers solve problems. Scientists previously would make a tremendous effort to simplify a complex problem to it's essence by reducing geometry, neglecting changes and only preserving first-order effects. Now, scientist are able to leave the details in the problem and computationally arrive at a result. To develop the computational physics programs used by scientists, developers make assumptions and use approximation to reduce complex, continuous calculus to algebraic expressions which computers are able to solve. While current computing technology is only capable of solving algebraic expressions, they are able to solve these expressions very rapidly making them immensely useful tools in research. However, it is important to be able to verify that the approximations and assumptions used by developers to create computational programs were not violated by the particular problem being solved. Further, it is important to verify results to ensure the user did not make an error in the input of the problem. The most essential tool to verify computational results is comparison to experiment. Sometimes, experimental data does not exist to compare to computational results requiring the need for an alternative method to verify computational results. This proposal develops a methodology used to appropriately apply the Boltzmann transport equation for neutrons (BTE) to sub-regions of a HI-STORM 100 spent fuel cask in order to verify MCNP simulation results of neutron transport through the cask. As the BTE is only solvable for the simplest of cases, a mathematical tool, symmetry analysis, will be introduced. Symmetry analysis provides a standardize approach for identifying symmetries present in partial differential equations to reduce the order of the differential equation. A sensitivity analysis of nuclear theory used in this work will also be proposed. Sensitivity analysis identifies the parameters that contribute the most to uncertainty in the system response. Establishing knowledge of key parameters can guide future model development to decrease the uncertainty of the result. Progress has been made in identifying a region to compare simplified analytic solutions and computational results. Initial results show agreement between the the two results, showing utility of the methodology. Continuing forward, more sub-regions will be identified and compared with appropriate analytic models solved using symmetry analysis. Afterward, a sensitivity study of nuclear theories used in this work will be conducted to identify parameters with the greatest affect on the system. The final goal of this research is to provide a complete methodology which can be used to verify computational results through comparison to analytic models with a reduced degree of mathematical complexity.

Contents

1 Introduction

This research explores the novel intersection of three seemingly disparate areas of physics and applied mathematics: neutron transport theory, symmetry or Lie group analysis techniques, and sensitivity analysis.

Generally speaking, a goal of this work is to seek sub-regions of a detailed problem (that otherwise can only be solved using numerical techniques) that are adequately described by the neutron transport equation. Depending on the specific choice of sub-region (in time, space, energy, or angle) additional simplifications of the neutron transport equation may be possible. The end goal of this exploration is to identify several problem sub-regions that are describable by mathematical models with a reduced degree of mathematical complexity, as opposed to that corresponding to the full-scale problem.

Simplified models corresponding to specific problem sub-regions may be described by systems of integro-differential equations, partial differential equations, ordinary differential equations, or algebraic equations, supplemented in some cases by initial, boundary, or ancillary conditions. Depending on the complexity of the simplified models, various forms of semi-analytic or even exact solutions may become possible. Symmetry analysis techniques are immensely valuable in this context, as they represent the most complete theory for systematically constructing broad classes of solutions, many of which possess special or otherwise desired properties (e.g., invariance under a variety of physical transformations such as translation, scaling, etc). As such, a primary focus of this work will be to use symmetry analysis methods to construct solutions for simplified sub-region models appearing within the broader problem framework, and provide comprehensive evaluation of the physical nature of these solutions.

Once solutions to the simplified models are obtained, they may be used for a variety of purposes. The principal aim of this research is comparison of the analytic solution models to computational simulation results arising from simulation of either the full scale problem, or the specific sub-regions. This procedure is phenomenological in nature, and is thus intended to capture elemental physical processes that are occurring within sub-regions of the full scale system. Therefore, while no analytic solution is expected to be available for the full scale system, any understanding gained in the sub-regions reinforces confidence that the integrated scales are being simulated in accordance with physical intuition. This outcome is extremely valuable in cases where experimental data is sparse or nonexistent.

In this work, the process of quantifying comparisons between the analytic and simulated models is exemplified through the inclusion of sensitivity analysis procedures. Forward modeling of sensitivity structures is conceptually simple but computationally expensive for large problems, as it involves sampling a space of possible parameter values and executing a new simulation for each value. For analytic models the procedure is the opposite: using a generalized notion of the directional derivative, sensitivity structures can often be computed in closed-form. The comparison of these two methods forms the final component of this work. In addition to basic physics phenomenology, the sensitivity structure arising from analytic models can be compared to that found from forward sensitivity modeling of full-scale simulations. When these structures compare favorably, confidence in the full-scale simulations is once again reinforced.

All of the above represents a generic procedure that can be applied to any physical system governed by systems of differential equations containing parameters. As a proof of principle with important applications, the emphasis of this work will

include analysis of a Holtec HI-STORM 100 spent nuclear fuel canister, as described in Sec. 2.1, through the previously described procedures. The principal physics describing the operation of this system is neutron transport, as briefly summarized in Sec. 2.2. Fundamentals of symmetry analysis and forward sensitivity analysis techniques are provided in Secs. 2.3 and 2.4, respectively.

1.1 Motivation

Simulation has become an important tool in research. Before the advent of supercomputing, problems had to be overly simplified before being solved. Now, we are able to solve much more complex problems to understand the physics occurring through use of simulation tools. While we do not need to simplify the problem as much to understand it, we still need to check that we have worked within the assumptions and approximations of the computational software or if an error was made by the user in the input file. The most essential tool to work this problem is comparison to experiment or comparison to other experiments that share similar features.

However, if no experimental data is available, we can use analytic or semi-analytic tools to check that we worked within the problem assumptions and approximations of the computational program. The purpose of my work is to compare analytic models, developed from theory, with computational results for the purposes of verifying that a simulation was conducted appropriately while simultaneously teaching the user about underlying physics in a problem. If the analytic solution agrees with the computational results, then the user's understanding of the underlying physics of the problem is correct and they are capable of analyzing the problem appropriately. However, the situation where the analytic solution and computational result differ can lead to an even more profound result. In this scenario, the user learns that either important physics was neglected or an error was made during analysis. In this case, the analytic solution has provided insight into the computed problem since the assumptions used to arrive at the analytic solution deepen the user's understanding of the physics occurring in a sub-region. In both situations, the user was able to learn about the underlying physics of the problem which leads to a more in depth and meaningful analysis of the results.

2 Background

To show the utility of verifying the correctness of a simulation, we investigate how nuclear theory can be applied to a spent fuel cask to aid in analysis. We begin by identifying a spent fuel cask and discussion of mathematical concepts of neutron transport, symmetry analysis, and sensitivity analysis.

2.1 Spent Fuel Casks

As a result of the halted promise of a permanent spent nuclear storage facility at Yucca Mountain, nearly 100 nuclear reactors face the question of how to store their growing amounts of used nuclear fuel. Cooling ponds are nearing capacity, or in some cases, at capacity. To store used nuclear fuel, power plants are building intermediate storage facilities until a permanent solution can be found. These intermediate storage facilities use dry fuel casks to provide environmental protection,

theft protection, and heat conduction for used fuel that has spent, at least, five years in a cooling pond. It is important that a cask is capable of performing these functions until a permanent solution is found.

Beyond acting as a radiation shield, casks are also designed with security features to show evidence of tampering in the event someone tries to remove fuel. In the event a tamper evident tag or seal is broken, the contents of the cask must be verified. Currently, a company would have to re-open the cask and visually verify that all fuel is accounted for before re-sealing the cask, an expensive endeavor. However, work by Dr. Greulich, among others, has been focused on non-destructive methods to verify cask contents using simulation as a basis for proof of concept [1, 2].

Simulation has proven a useful tool for ensuring spent fuel casks are capable of providing environmental, theft, and radiation protection. Unfortunately, experimental data for which theses simulations can be compared is limited, and in some cases, non-existent. Motivating the need for verification tool to ensure the correctness of spent fuel cask simulation results.

This work investigates a Holtec HI-STORM 100 canister system to develop a methodology to as a process of quantifying comparisons between the analytic and simulated models. This cask is the most used dry cask system currently implemented [3]. Holtec designed the HI-STORM 100 system to hold spent fuel from pressurized water reactors (PWR) or boiling water reactors (BWR) in an inner multi-purpose canister (MPC), see figure 1 [4]. Spent fuel rods are inserted into fuel cells as bundles of rods and steel structure.

The MPC is designed with an inner, honeycomb structure to hold the fuel rods, provide radiation shielding, and conduct heat away from spent fuel. A neutron absorber, Boral^{TM}, is placed in key locations within the honeycomb basket where the locations vary based on the type of MPC. Boral^{TM} is a combination of boron carbide (B_4C) powder filling the space between two aluminum plates. The MPC is backfilled with helium to purge the system before being sealed shut. Figure 2 shows the three types of MPC basket structures used with the HI-STORM 100 system, where the number in the name corresponds to the number of cells in the basket. The MPC-24 and 32 are used to store PWR spent fuel where the MPC-68 has been designed to store BWR fuel. The MPC-32 was chosen to demonstrate the principals in this work, but the methodology developed by this work is capable of being extended to other MPC designs.

The HI-STORM 100 storage overpack is a combination of standard concrete surrounded by a shell of carbon steel which stands around 600 cm tall and about 335 cm in diameter, fig. 3. The overpack has inner channels to provide natural convection between the MPC and the environment. A 75 cm thick annulus of concrete surrounds the MPC to provide neutron shielding and protection in the event the cask falls or tips over. A radial layer of carbon steel surrounds the concrete to provide gamma shielding and to increase the integrity of the cask in the event of the cask was dropped or tipped over. The overpack has neutron and gamma shielding beneath the MPC (the pedestal) and above the MPC (the lid) which are comprised of the same materials to ensure proper joining of the casks seals.

The HI-STORM 100 canister system as designed to be used as part of the larger HI-TRAC system. The HI-TRAC system is used to transfer canisters to the intermediate storage site or to a future permanent storage location. This work investigates a HI-STORM 100 canister system sitting on an independent spent fuel storage installation, therefor, the HI-TRAC transportation shielding will not be investigated in this work.

Spent fuel generates a mixed spectrum of neutrons and gammas which the

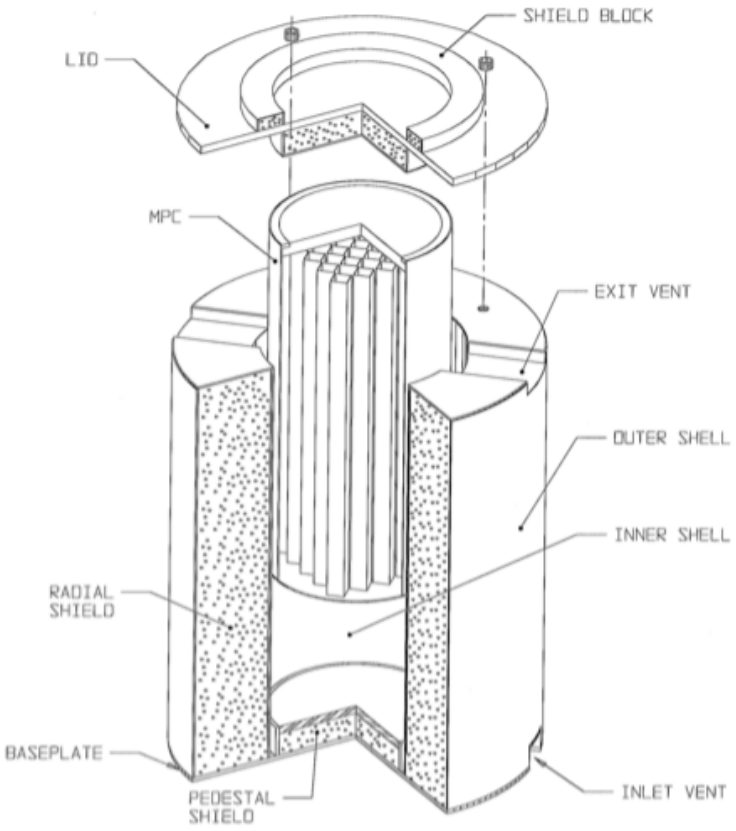

Figure 1: Section view of Holtec HI-STORM overpack with MPC.

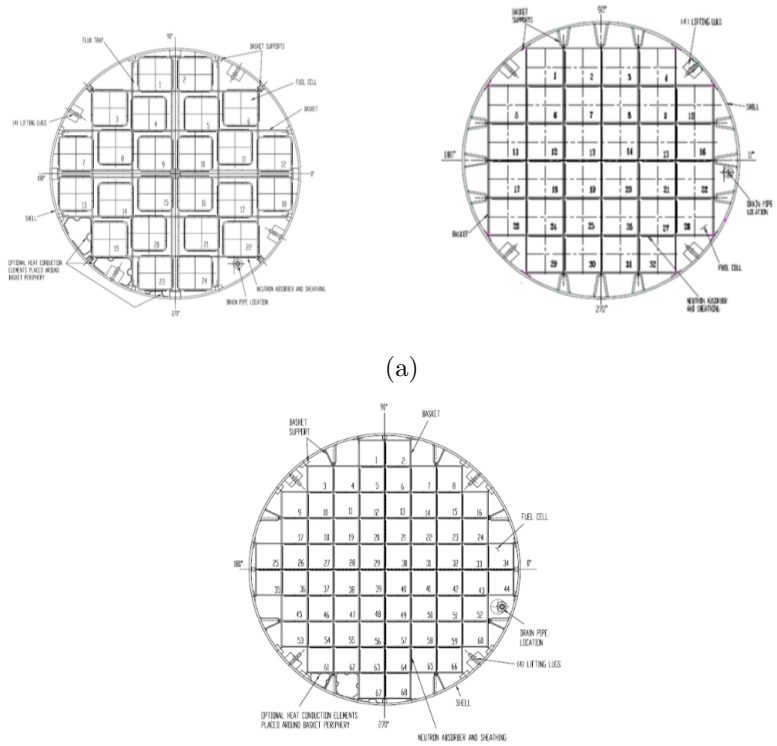

(a) (b)

(c)

Figure 2: Three MPC configurations used with the Holtec HI-STORM 100. a) MPC-24, b) MPC-32, c) MPC-68. The MPC-32 was chosen for this work.

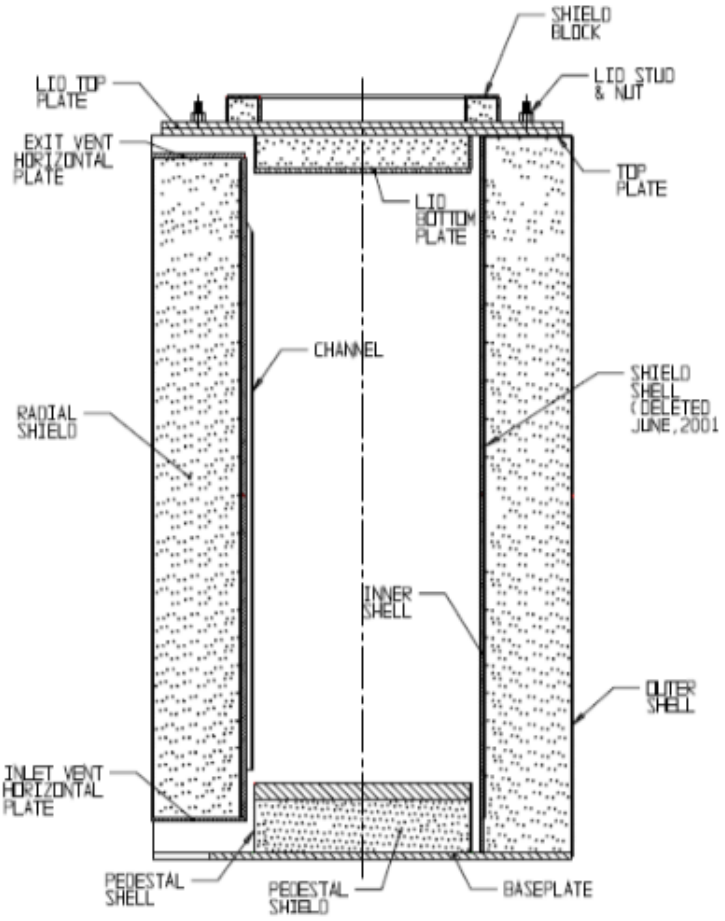

Figure 3: Holtec HI-Storm 100 overpack. The central annulus is standard concrete to provide neutron shielding and protection if the cask were dropped or tipped over. The concrete is surrounded by carbon steel to provide gamma shielding, strength, and protection.

HI-STORM 100 spent fuel casks attenuates to provide radiation shielding to power plant workers and surrounding public. For this work, the transport of neutrons through the spent fuel cask will be investigated. The Boltzmann transport equation (BTE) for neutrons mathematically describes the transport of neutrons through matter, and forms the basis for the analytic models used in this work.

2.2 Neutron Transport

The BTE, also called the neutron transport equation, describes the population density of neutrons in a given environment and was developed as a balance equation accounting for the neutrons in a particular region of phase spaced given by $dV, dE, d\hat{\mathbf{\Omega}}$, and dt. dV is an incremental volume, dE is an incremental energy, $d\hat{\mathbf{\Omega}}$ is the incremental direction vector, and dt is an incremental time. Time dependence will be neglected for this work as the neutron spectrum evolves slowly in time compared to the time between neutron interactions. We use a heuristic approach to develop the BTE accounting for source and loss terms [5]. We will begin by mathematically creating expressions for each of the following terms:

I Gain Mechanisms

(a) All neutron sources in volume dV

(b) Neutrons streaming into volume dV, through an incremental surface dS

(c) Neutrons in a different phase space entering the phase space of interest

II Loss Mechanisms

(d) Neutrons leaking out through surface dS

(e) Neutrons undergoing a reaction in dV

Duderstadt and Hamilton provide a framework for transforming the heuristic expression into an equation [6]. Starting with the most straight-forward terms and progressively getting more difficult, we take the source term, term (a),

$$(a) = \left[\int_V s(\boldsymbol{r}, E, \hat{\mathbf{\Omega}}) d^3r \right] dE d\hat{\mathbf{\Omega}} = S(\boldsymbol{r}, E, \hat{\mathbf{\Omega}}). \tag{1}$$

Eqn. 1 describes the neutrons generated in dV, where $\boldsymbol{r}$ is the position vector that describes the center point of dV. The source term accounts for all neutrons with energy in range E to $E + dE$ produced from an external source such as fission or radioactive decay.

A neutron can be removed from our phase space as a result of an interaction. Eqn. 2 accounts for neutrons lost through interactions. Σ_t is the total macroscopic cross section. Cross sections determine the probability of a certain type of reaction occurring. The total cross section determines the probability of any reaction occurring. φ is the neutron angular flux, the variable for which we will be solving. The flux describes the neutron population as a function of $\boldsymbol{r}, E, \hat{\mathbf{\Omega}}$ and is used in many areas of nuclear engineering, such as in calculating dose to a person, detecting illicit material, and determine burn-up of nuclear fuel.

$$(e) = \left[\int_V \Sigma_t(\boldsymbol{r}, E) \varphi(\boldsymbol{r}, E, \hat{\mathbf{\Omega}}) d^3r \right] dE d\hat{\mathbf{\Omega}} \tag{2}$$

The in-scattering term, term (c), accounts for neutrons scattering from other energies or directions into $dE d\hat{\mathbf{\Omega}}$. Mathematically, this process is expressed as

$$(c) = \int_V d^3r \int_{4\pi} d\hat{\mathbf{\Omega}} \int_0^\infty dE' \Sigma_s(E' \to E, \hat{\mathbf{\Omega}}' \to \hat{\mathbf{\Omega}}) \varphi(\boldsymbol{r}, E', \hat{\mathbf{\Omega}}). \tag{3}$$

Σ_s is the macroscopic scattering cross section. This value determines the probability a neutron will undergo a scattering event, which will change the neutron's direction and can change the neutron's kinetic energy. The integration over the primed quantities indicates a neutron can enter the appropriate point in phase space from any other direction or energy.

Terms (b) and (d) together describe the neutron streaming in dV. Taking

$$(d) - (b) = \int_V d^3r \hat{\mathbf{\Omega}} \cdot \varphi(\boldsymbol{r}, E, \hat{\mathbf{\Omega}}) \tag{4}$$

to be the mathematical expression derived by using divergence theorem to convert the boundary integral into a volume integral to determine the net number of neutrons entering dV.

To handle the integral over dV, we apply the fact that the volume was chosen arbitrarily. Hence, the only way for the integral to vanish for any volume is for the integrand to equal zero [6]. We arrive at the BTE

$$\hat{\mathbf{\Omega}} \cdot \boldsymbol{\nabla} \varphi + \Sigma_t(\boldsymbol{r}, E) \varphi(\boldsymbol{r}, E, \hat{\mathbf{\Omega}}) = \int_{4\pi} d\hat{\mathbf{\Omega}}' \int_0^\infty dE' \Sigma_s(E' \to E, \hat{\mathbf{\Omega}}' \to \hat{\mathbf{\Omega}}) \varphi(\boldsymbol{r}, E', \hat{\mathbf{\Omega}}) + S(\boldsymbol{r}, E, \hat{\mathbf{\Omega}}). \tag{5}$$

The BTE is a linear, first-order, integro-differential equation, one of the most difficult forms of problems to solve. The solution to the full BTE can only be found in the simplest of cases. Current work uses a reduced form of the BTE to solve for the flux across a slab of Boral^{TM} near the center of the cask. Discussion of the assumptions used to arrive at a tractable form of the BTE are found in Sec. 3.4. Understanding which assumptions on the analytic model hold reveals underlying physics of the problem. If the simplified analytic solution matches the simulated result, the assumptions applied to the analytic solution were valid and we understand the physics in that sub-region. However, if the analytic solution does not match the simulated result, we now understand that there is some physics not being accounted for in the analytic model. In either situation, we have learned more about the physics of the problem.

Future work will relax the assumptions currently used to arrive at a manageable analytic model, resulting in models that more accurately describe the underlying physics of a problem. Solving future models is expected to require the use of more robust differential equation solving methods. Symmetry analysis is a technique that reduces the complexity of a differential equation, resulting in a more tractable expression.

2.3 Symmetry Analysis

Current work is focused on applying analytic models to sub-regions in phase space. These analytic models prove challenging to solve directly and therefore require some type of simplifications to solve. In order to reduce the complexity of the models used in this work, assumptions were applied. Applying assumptions, however, results in a loss of accuracy. Therefore, it would be beneficial to relax assumptions used in initial work to arrive at more rigorous analytic models. Methods do exists for solving these equations, but many methods rely on manipulating a differential equation

into a form for which a solution is already known. This can become cumbersome or impossible as the difficulty of an equation increases, these methods may not be able to be applied. Symmetry analysis provides a more standardized approach to solving linear and non-linear differential equations. As symmetry techniques will become important in future work, it is convenient to introduce a framework at this point.

Symmetry analysis is essentially the systematic means for constructing a change of variables that maps a differential equation into a space where the equation depends on fewer variables. The solutions to the simplified problem will also be solutions to the original differential equation if the differential equation is invariant under a chosen transformation process.

Mathematical invariance occurs when a transform is applied to an equation which leaves the equation unchanged in a new coordinate system [7]. To further explain invariance, the following example is provided. $F(x, y, \frac{\partial y}{\partial x})$ is the function described by x, y and $\frac{\partial y}{\partial x}$, eqn. 6.

$$F\left(x, y, \frac{\partial y}{\partial x}\right) = \frac{\partial y}{\partial x} - e^{x-y} = 0 \tag{6}$$

Introducing the translation operation on x, y, and $\frac{\partial y}{\partial x}$ as

$$\begin{aligned} x &= \tilde{x} + s \\ y &= \tilde{y} + s \\ \frac{\partial y}{\partial x} &= \frac{\partial \tilde{y}}{\partial \tilde{x}}. \end{aligned} \tag{7}$$

Substituting the expressions for x, y, and $\frac{\partial y}{\partial x}$ into eqn. 6 leaves the original function invariant as shown by eqn. 8.

$$\begin{aligned} F\left(x, y, \frac{\partial y}{\partial x}\right) &= \frac{\partial y}{\partial x} - e^{x-y} \\ &= \frac{\partial \tilde{y}}{\partial \tilde{x}} - e^{\tilde{x}+s-(\tilde{y}+s)} = F\left(\tilde{x}, \tilde{y}, \frac{\partial \tilde{y}}{\partial \tilde{x}}\right) \end{aligned} \tag{8}$$

Function $\tilde{F}$ is the transformed function. The important piece to note is the elimination of the constant, s, as a result of the transformation. The expressions we are interested in will be invariant under certain transformations which will lead to a reduction of one or more independent variables resulting in a more tractable problem.

A transformation that maps a function onto itself, ie. leaves the function invariant, is called a symmetry. Since all points of the original function are mapped back onto itself, the solutions of $\tilde{F}$ are then solutions of F. If $\tilde{F}$ is simplified by the transformation, then determining the solutions to $\tilde{F}$ will be a simpler endeavor than solving F directly. Symmetry analysis is a useful tool to solve difficult ordinary and partial differential equations, however, finding the symmetries exhibited by an equation is not a trivial task. Luckily, some symmetries can be found systematically where the resultant set of symmetries are helpful in solving systems of autonomous ordinary differential equations [8]. We will now determine the symmetries of a first-order differential equation using methods presented by Olver to examine the utility of symmetry analysis in solving a complex differential equation [9].

Taking an additional example

$$G\left(x, y, \frac{dy}{dx}\right) = \frac{dy}{dx} - \frac{y}{x} - tan\left(\frac{y}{x}\right) = 0. \tag{9}$$

Eqn. 9 has no immediately apparent solution. Determining symmetries through inspection proves challenging as well. Therefore, we must systematically identify the symmetries for this problem.

To provide a general basis for symmetry analysis techniques, we take an arbitrary function, $F(x, y, \frac{dy}{dx})$ and relabel $\frac{\partial y}{\partial x}$ as z, for notation simplicity, before returning to our example given in 9.

We begin by defining a set of transformations under which $F(x, y, z)$ is invariant.

$$\tilde{x} \coloneqq \alpha(x, y, z; \epsilon), \qquad \tilde{y} \coloneqq \beta(x, y, z; \epsilon), \qquad \tilde{z} \coloneqq \gamma(x, y, z; \epsilon) \tag{10}$$

In our transformations, ϵ represents the group parameter used to transform x, y and z to $\tilde{x}, \tilde{y}$ and $\tilde{z}$ and α, β, and γ are arbitrary functions that transform x, y and z.

Using the set of transformations in 10, lead to:

$$F(\tilde{x}, \tilde{y}, \tilde{z}) = F(x, y, z) \tag{11}$$

For clarity, we will redefine $F(x, y, z)$ as F and $F(\tilde{x}, \tilde{y}, \tilde{z})$ as $\tilde{F}$. We want to deduce the linearized action of the transformation about the identity element on F. We do this because evaluating eqn. 11 for arbitrary α, β, γ is difficult if not impossible. Lie's great achievement was demonstrating that this localized evaluation of 11 is entirely adequate to determine invariance. The identity transformation, I, is defined as an operator that acts on a function to yield the same function,

$$I\{F\} = \tilde{F} = F. \tag{12}$$

Taking the Taylor series expansion about $\epsilon = 0$

$$\tilde{F} = F + \epsilon \frac{\partial \tilde{F}}{\partial \epsilon}\Big|_{\epsilon=0} + \frac{\epsilon^2}{2} \frac{\partial^2 \tilde{F}}{\partial \epsilon^2}\Big|_{\epsilon=0} + \mathcal{O}(\epsilon^3). \tag{13}$$

Using chain rule to compute the derivative of the linear term yields

$$\frac{\partial \tilde{F}}{\partial \epsilon} = \frac{\partial F}{\partial \alpha}\frac{\partial \alpha}{\partial \epsilon} + \frac{\partial F}{\partial \beta}\frac{\partial \beta}{\partial \epsilon} + \frac{\partial F}{\partial \gamma}\frac{\gamma}{\partial \epsilon}. \tag{14}$$

Evaluating at $\epsilon = 0$ and defining

$$\eta = \frac{\partial \alpha}{\partial \epsilon}\Big|_{\epsilon=0}, \qquad \phi = \frac{\partial \beta}{\partial \epsilon}\Big|_{\epsilon=0}, \qquad \zeta = \frac{\partial \gamma}{\partial z}\Big|_{\epsilon=0}, \tag{15}$$

leads to

$$\frac{\partial \tilde{F}}{\partial \epsilon}\Big|_{\epsilon=0} = \Big[\eta \frac{\partial}{\partial x} + \phi \frac{\partial}{\partial y} + \zeta \frac{\partial}{\partial z}\Big] F. \tag{16}$$

Determining the derivative of the second order term in eqn. 13 results in

$$\begin{aligned} \frac{\partial^2 \tilde{F}}{\partial \epsilon^2} &= \frac{\partial}{\partial \tilde{x}}\Big(\frac{\partial F}{\partial \epsilon}\Big)\frac{\partial \tilde{x}}{\partial \epsilon} + \frac{\partial}{\partial \tilde{y}}\Big(\frac{\partial F}{\partial \epsilon}\Big)\frac{\partial \tilde{y}}{\partial \epsilon} + \frac{\partial}{\partial \tilde{z}}\Big(\frac{\partial F}{\partial \epsilon}\Big)\frac{\partial \tilde{z}}{\partial \epsilon} \\ &= \Big[\frac{\partial}{\partial \tilde{x}}\frac{\partial \tilde{x}}{\partial \epsilon} + \frac{\partial}{\partial \tilde{y}}\frac{\partial \tilde{y}}{\partial \epsilon} + \frac{\partial}{\partial \tilde{z}}\frac{\partial \tilde{z}}{\partial \epsilon}\Big]\frac{\partial F}{\partial \epsilon}. \end{aligned} \tag{17}$$

Evaluating eqn. 17 at $\epsilon = 0$ yields

$$\frac{\partial^2 \tilde{F}}{\partial \epsilon^2}\Big|_{\epsilon=0} = \Big[\eta \frac{\partial}{\partial x} + \phi \frac{\partial}{\partial y} + \zeta \frac{\partial}{\partial z}\Big]\Big[\eta \frac{\partial}{\partial x} + \phi \frac{\partial}{\partial y} + \zeta \frac{\partial}{\partial z}\Big] F. \tag{18}$$

The solutions to the first and second order terms share a common factor of $\eta\frac{\partial}{\partial x}+\phi\frac{\partial}{\partial y}+\gamma\frac{\partial}{\partial z}$. From inspection, it can be seen that higher order terms of eqn. 13 will depend on $\eta\frac{\partial}{\partial x}+\phi\frac{\partial}{\partial y}+\gamma\frac{\partial}{\partial z}$ as well. This term is called the prolonged group generator which we defined as

$$pr\mathbf{X} \coloneqq \eta\frac{\partial}{\partial x}+\phi\frac{\partial}{\partial y}+\zeta\frac{\partial}{\partial z}. \tag{19}$$

Using the prolonged group generator to rewrite eqn. 13 results in

$$\tilde{F} = F+\epsilon pr\mathbf{X}F+\frac{\epsilon^2}{2}pr\mathbf{X}^2F+\mathcal{O}(\epsilon^3). \tag{20}$$

Subtracting F from both sides yields

$$\tilde{F}-F = \epsilon(pr\mathbf{X}F)+\frac{\epsilon^2}{2}pr\mathbf{X}(pr\mathbf{X}F)+\mathcal{O}(\epsilon^3). \tag{21}$$

To find symmetries exhibited by F and to find where F is invariant, we need to solve eqn. 21 when set equal to 0. Luckily, $(pr\mathbf{X}F)$ is in every term of eqn. 21. Therefore, wherever $(pr\mathbf{X}F)=0$ holds, all terms of eqn. 21 are simultaneously 0.

We return to our example problem, 9, and apply the prolonged group generator, eqn. 19 which allows us to solve for η,ϕ and ζ. Taking the derivatives results in the determining equation, eqn. 22.

$$\eta\Big[\frac{y}{x^2}+\frac{y}{x^2}sec^2\left(\frac{y}{x}\right)\Big]+\phi\Big[\frac{1}{x}+\frac{1}{x}sec^2\left(\frac{y}{x}\right)\Big]+\zeta=0 \tag{22}$$

Through inspection, a solution to the determining equation is

$$\eta = x, \qquad \phi = y, \qquad \zeta = 0. \tag{23}$$

We need to ensure the definition of the derivative is preserved (invariant) across the coordinate transform. We can check that the derivative is invariant under the transform by setting z equal to zero, and using the definition of z, as

$$z-\frac{dy}{dx} = z(dx)-dy = 0. \tag{24}$$

Applying the prolonged group generator to check for invariance yields

$$pr\mathbf{X}(z(dx)-dy)=0. \tag{25}$$

Evaluating eqn. 25 using chain rule gives

$$zpr\mathbf{X}(dx)+dxpr\mathbf{X}(z)-pr\mathbf{X}(dy)=0. \tag{26}$$

Remembering eqn. 19 and using the identity $pr\mathbf{X}(dx)=d\big(pr\mathbf{X}(x)\big)$ to evaluate eqn. 26 leads to

$$\zeta+\left[\frac{\partial\eta}{\partial x}+\frac{\partial\eta}{\partial y}z\right]z-\left[\frac{\partial\phi}{\partial x}+\frac{\partial\phi}{\partial y}z\right]=0. \tag{27}$$

Using 23 to verify eqn. 27 is equal to 0,

$$0+[1+0z]z-[0+z]=0. \tag{28}$$

After verifying the accuracy of the prolonged group generator, values for η,ϕ, and ζ are substituted into eqn. 19. Since the value of ζ is 0, the prolonged group

generator is reduced to the group generator, $\mathbf{X}$. The difference being the group generator does not contain information about derivatives where the prolonged group generator contained information about z. The final expression for the group generator is

$$\mathbf{X} = x\frac{\partial}{\partial x} + y\frac{\partial}{\partial y} \tag{29}$$

We now apply $\mathbf{X}$ to a function $F(x, y)$ which we want to exhibit the same symmetries as our differential equation. To accomplish this, we set $\mathbf{X}\{F\} = 0$.

$$\mathbf{X}\{F\} = x\frac{\partial F}{\partial x} + y\frac{\partial F}{\partial y} = 0 \tag{30}$$

We have now produced the characteristic system,

$$\frac{dF}{0} = \frac{dx}{x} = \frac{dy}{y}. \tag{31}$$

Solving the characteristic system yields a set of constants, called similarity variables, which will be a combination of dependent and independent variables that do not change under the action of the group. These constants can then be used to simplify our differential equation.

$$\frac{dF}{0} = \frac{dx}{x} \tag{32}$$

and

$$\frac{dx}{x} = \frac{dy}{y} \tag{33}$$

produces

$$F = constant \tag{34}$$

and

$$r = \frac{y}{x}, \tag{35}$$

from eqns. 32 and 33 respectively. r is the similarity variable arising from the solution to the characteristic system.

We still need to determine $\frac{dy}{dx}$ in the new coordinate system. This is done by applying chain rule to eqn. 35, where the result is given by

$$\frac{dy}{dx} = \frac{d}{dx}(rx) = \frac{dr}{dx}x + r. \tag{36}$$

We can now rewrite eqn. 9 into our new coordinate system using r,

$$\frac{dr}{dx}x + r - r - tan(r) = \frac{dr}{dx}x - tan(r) = 0. \tag{37}$$

Eqn. 37 is a separable equation with the solution

$$r = sin^{-1}(cx) \tag{38}$$

where c is an integration constant. Finally, mapping eqn. 38 back into our original coordinate system produces the solution to eqn. 9,

$$y = xsin^{-1}(cx). \tag{39}$$

To summarize the symmetry analysis method:

1. Re-write $F(x, y, \frac{dy}{dx})$ as $F(x, y, z) = 0$.
2. Apply the group generator to set up the determining equations.
3. Solve the determining equations to find the values for η, ϕ, and ζ.
4. Apply the completed prolonged group generator to find the characteristic system.
5. Solve the characteristic system to find the similarity variables.
6. Re-express F in terms of the similarity variables to arrive at a simplified expression.
7. Solve the simplified expression in terms of the similarity variables.
8. Re-express the solution in the original coordinate system.

The process of determining symmetries is time intensive and lends itself to many mathematical errors. Luckily, there are mathematical software packages that streamline the steps to acquiring the determining equations. These software tools will likely be used in future work to aid in solving complicated analytic models.

2.4 Sensitivity Analysis

Once the validity of analytic models is established, sensitivity analysis will be performed to rank the affect of uncertainty values inherent to the parameters present in our models. The framework for sensitivity analysis is general allowing it to be applied to the equations which approximate neutron transport.

A physical system is modeled by linear and/or non-linear equations which define the systems response to a given input based on parameters. These parameters are not classified as independent nor dependent variables, rather, proportionality constants, physical constants, and derived quantities are among the the list of possible categories of parameters.

In many cases, these parameters are regarded as constants with presumably fixed values. In other cases, there is a level of uncertainty attached to a parameter, with this uncertainty being described by a standard deviation with respect to some mean of a set of measured values. This is the cases often found in models of physical systems containing experimentally measured parameters, such as cross section data in the context of neutron transport.

It becomes important to be able to predict the response of a particular mathematical model to the behavior of input parameters. The practice of ascertaining the behavior of a system in response to input parameter variations in known as sensitivity analysis. The goal of sensitivity analysis is to analyze the behavior of the response around a point or trajectory in the phase space defined by the parameters and state variables of a problem [10].

The mathematical development of sensitivity analysis has been complied in exacting detail in a purely mathematical setting by a number of authors including Saltelli, et al.[11], Turányi & Rabitz [12], and Cacuci [13, 14]. Many of these methods require extensive computational resources. However, Cacuci identified a direct correspondence between the concepts of local sensitivity analysis (quantifying the affects of small perturbations around a nominal parameter value) and a mathematical entity known as the Gâteaux-derivative (G-derivative). From this association, he circumvented many of the drawbacks inherent to traditional local sensitivity analysis.

Cacuci's development is also more general than alternatives, while allowing for analysis of models that are not easily handled using other techniques. Therefore, Cacuci's methods will be used in this work to perform sensitivity analysis.

To determine the sensitivities of a system's response, we introduce the G-derivative. The G-derivative is a generalization of a directional derivative and exists at discontinuities of a function as long as direction is continuous. Taking x_0 and t as real numbers, h is a fixed, nonzero element in real space, and $R(x_0)$ to be the system response at x_0, then the G-derivative of $R(x_0)$ is defined as:

$$\delta R(x_0; h) \coloneqq \lim_{t \to 0} \frac{R(x_0 + th) - R(x_0)}{t}. \tag{40}$$

Finding a system's sensitivities involves calculating the first G-derivative, therefore $\delta R(x_0; h)$ is the sensitivity of the response to variation, h. Cacuci develops two procedures for calculating a sensitivities: the Forward Sensitivity Analysis Procedure (FSAP) and the Adjoint Sensitivity Analysis Procedure (ASAP). The FSAP calculates the sensitivity of parameter variations individually. When the number of parameter variations becomes large, it become advantageous to use the ASAP procedure [15]. This method uses a solution of the FSAP along with the adjoint problem to solve the sensitivities of all parameters simultaneously. Proposed work will use the FSAP as the number of parameter variations being investigated is expected to be low enough that using the ASAP would not be advantageous.

2.4.1 Forward Sensitivity Analysis Procedure

Physical systems can be modeled by a system of coupled operator equations that can be mathematically expressed as

$$\boldsymbol{L}(\boldsymbol{\alpha})\boldsymbol{u} = \boldsymbol{Q}[\boldsymbol{\alpha}(x)]. \tag{41}$$

$\boldsymbol{L}$ is a column vector containing the operators that act on $\boldsymbol{u}$, the unique, nontrivial solutions of a physical problem. $\boldsymbol{\alpha}$ is a vector of parameters for the physical problem. $\boldsymbol{Q}$ contains the inhomogeneous source terms.

Boundary conditions are used to solve the set coupled differential equations in eqn. 41. We express the boundary conditions mathematically eqn. 41 as

$$\boldsymbol{B}(\boldsymbol{\alpha u} - \boldsymbol{A}(\boldsymbol{\alpha}). \tag{42}$$

$\boldsymbol{A}$ and $\boldsymbol{B}$ are operators, where $\boldsymbol{A}$ represents all inhomogeneous boundary terms.

The FSAP involves taking the G-derivative of both eqn. 41 and 42. The result of the respective G-derivatives is provided as eqn. 43 and 44.

$$\boldsymbol{L}(\boldsymbol{\alpha}^0)\boldsymbol{h}_u + \left[\boldsymbol{L}'_\alpha(\boldsymbol{\alpha}^0)\boldsymbol{u}^0\right]\boldsymbol{h}_\alpha - \delta\boldsymbol{Q}(\boldsymbol{\alpha}^0; \boldsymbol{h}_\alpha) = \boldsymbol{0} \tag{43}$$

$$\left\{\boldsymbol{B}(\boldsymbol{\alpha}^0)\boldsymbol{h}_u + \left[\boldsymbol{B}'(\boldsymbol{\alpha}^0)\boldsymbol{u}^0\right]\boldsymbol{h}_\alpha - \delta\boldsymbol{A}(\boldsymbol{\alpha}^0; \boldsymbol{h}_\alpha)\right\} = \boldsymbol{0} \tag{44}$$

$\boldsymbol{L}'_\alpha(\boldsymbol{\alpha}^0)$ and $\boldsymbol{B}'(\boldsymbol{\alpha}^0)$ denote the first-order, partial G-derivative of $\boldsymbol{L}$ and $\boldsymbol{B}$ with respect to $\boldsymbol{\alpha}$. Quantities with a zero superscript $(^0)$ are vectors containing values of the unperturbed system, the nominal values of the system. $\boldsymbol{h}_\alpha$ is the vector containing the parameter variations. $\boldsymbol{h}_u$ is a vector of the variations in the state functions contained in $\boldsymbol{u}$.

Luckily, the values of $\boldsymbol{h}_\alpha$ are known, since these parameter variations are chosen by the user. Solving the system of equations in eqn. 43 with boundary conditions, eqn. 44, will yield the variation in the state vector, $\boldsymbol{h}_u$.

The result of $\boldsymbol{h}_u$ is used to determine the affects of the variation of input parameters on the response of the system, the goal of our analysis. Knowing the importance of each parameter can guide future model development to decrease the uncertainty in the most important parameters and can also be used to reformulate models to include only the most important parameters, which would reduce computational resources needed to evaluate a problem [10, 16].

3 Current Work

Current work has been focused on developing a simplified HI-STORM 100 cask system using Monte Carlo N-Particle (MCNP) radiation transport code [17, 18]. Neutron transport is the focus of this work, however, the methodologies developed here can be extended to photon and charged particle transport. The MCNP geometry was used in identifying a sub-region where assumptions could be applied appropriately to develop a tractable analytic equation. These equations were then solved and compared to results of the MCNP simulations as a proof of concept.

3.1 MCNP Geometry

To model the HI-STORM 100 in mcnp, some simplifications had to be made to the MPC and overpack in order to reduce computation time required to converge simulation results. One simplification was to homogenize the fuel bundles in each cell of the fuel basket. Another was to eliminate some of the finer structure in the canister system, such as lifting rings and bolts used to move or secure the MPC and overpack. Figure 4 is the side view of the cross section of the HI-STORM overpack filled with the MPC-32.

Figure 5a is the top down cross section view of the HI-STORM 100 overpack and MPC-32. This view shows the homogenized fuel regions enclosed by the honeycomb lattice of the MPC fuel basket. Figure 5b is a view of one fuel cell, showing the fuel region surrounded by helium gas, all contained by the 304 stainless steel (304 SS) basket. This image also shows the location of the Boral^{TM} pads. These pads were also homogenized by weight as they were during the licensing of the MPC container [4].

Due to the complexity of the simplified cask, only $\frac{1}{8}$ of the cask was simulated. Figure 6 shows the final cask geometry used in MCNP simulations. The cask was cut in half along the vertical axis and radially into quarters. Reflective boundaries were used at each place the cask was cut to account for simplifying the geometry. Tallies were also added in the simulation for comparison between simulation and analytic results. An FMESH tally was applied across the Boral^{TM} slab to measure simulated flux through the pad.

3.2 Source Term

A realistic source spectrum was generated based on decay models from experimentally determined spent fuel compositions. The Next Generation Safeguards Initiative (NGSI) provides a detailed MCNP input desk for Westinghouse 17x17 PWR fuel with

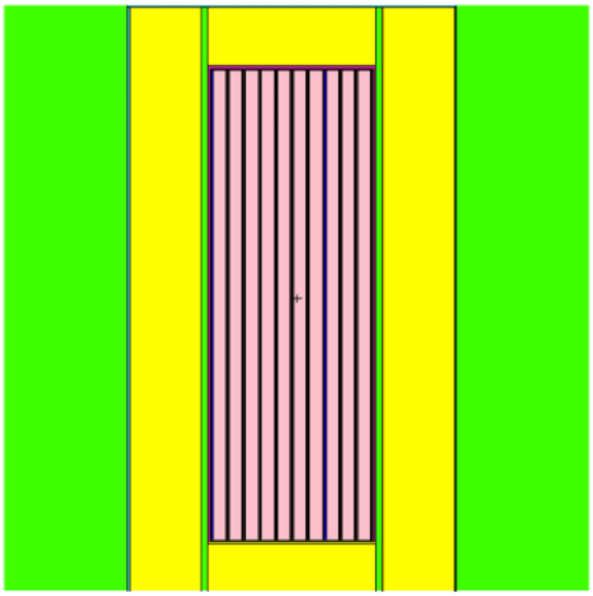

Figure 4: Cut away side view of the interior of the cask used in MCNP simulations. The thin blue edge at the outside of the cask is carbon steel. The yellow region is concrete with openings for outside air (green) to enter the interior of the cask for heat transfer purposes. The dark pink is the MPC filed with rectangular light pink colored fuel regions.

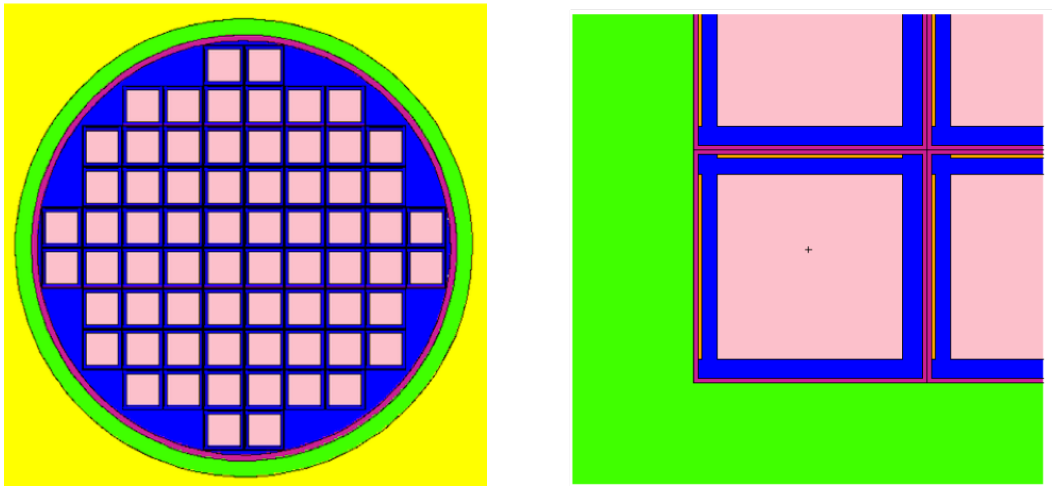

(a) (b)

Figure 5: a) The top down section view of the MPC-32 used in MCNP simulations. b) A single fuel cell region.

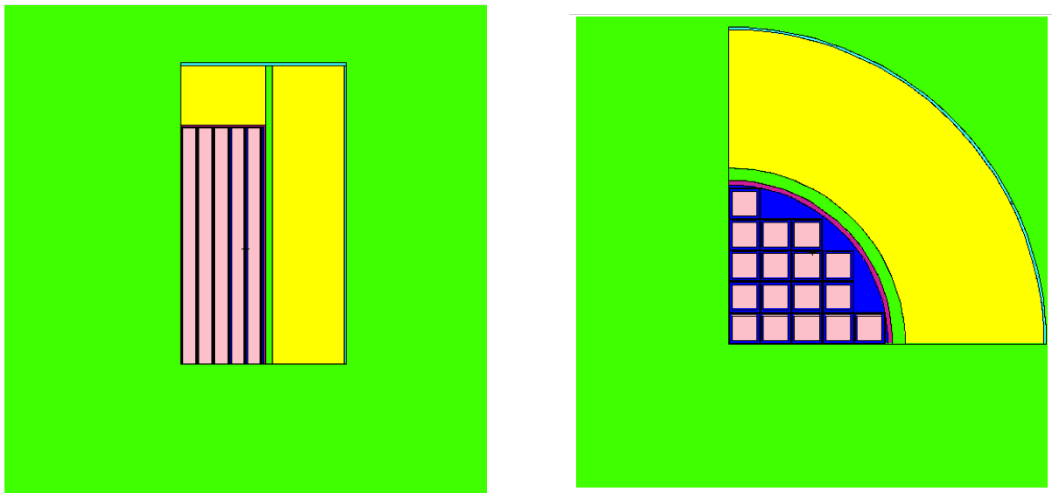

(a) (b)

Figure 6: The complexity of a full cask requires significant computational resources. Therefore, a $\frac{1}{8}$ cask was simulated in MCNP. a) Side view and b) top view of the $\frac{1}{8}$ cask used in simulations.

various initial enrichment and burn-up values [3]. Initial enrichment and burn-up of 3 wt% ^{235}U, 30 GWd/MTU respectively were chosen for this work, similar to work conducted by Yuan Gao [19]. Initial concentrations of each isotope were determined by running an initial MCNP simulation in initialization only mode based on data provided by NGSI. Once the initial concentrations were found, an ORIGEN-S input deck was developed to calculate the spectrum as a result of spontaneous fission and [α,n] reactions, the two predominate sources of neutrons from spent fuel [20]. ORIGEN-S is a 0-dimensional irradiation and decay modeling code included in the SCALE packages developed by Oak Ridge National Lab [21]. The input deck used to determine the neutron spectrum was based on work by Bowman [22]. The fuel was cooled for 11 years before determining the neutron spectrum, similar to work performed by Yuan Gao [19]. The spectrum is provided in figure 7.

3.3 Choice of Sub-region

A single fuel cell was chosen to be the sub-region of interest for initial proof of concept calculations. In the analytic models of the fuel cell, He gas was treated with a free-streaming approximation, the homogenized fuel acted as the source and transport was conducted through the Boral^{TM} slab. The following sections discuss the reasoning for handling the fuel cell in the manner which it was treated.

3.4 Choice of Analytic Model

Qualitative analysis of the fuel cell alluded to the use of either diffusion equation or a simplified BTE (resulting from applying assumptions). However, the accuracy of initial qualitative conclusions needed to be tested to arrive at a final model.

An initial check was performed by comparing the total cross section of Boral^{TM} and He to the source flux from the spent fuel. Figure 8 shows that the contribution of thermal neutrons on the total will be small, since the source flux decreases

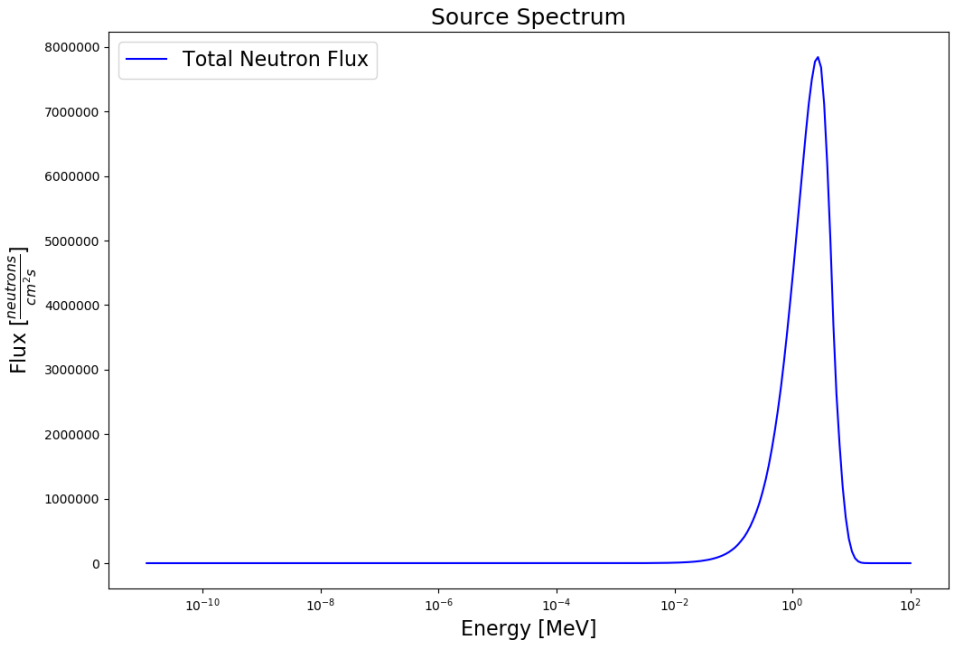

Figure 7: The source spectrum used in the MCNP simulation. This spectrum was generated using ORIGEN-S to determine the neutron spectrum from 3 % enriched Westinghouse 17x17 PWR spent fuel burned to 30 GWd/MTU.

approximately two orders of magnitude below 1 MeV. However, since the cross section of Boral^{TM} increases at thermal neutron energies, a two-group model was decided upon to handle the separate physics that occurs at different neutron energies.

After deciding to handle the energy dependence as two separate energy groups, a transport model had to be chosen. Figure 9 aided in the selection of a simplified BTE model. Figure 9 shows the mean free path (mfp) of the materials of interest between the fuel region and Boral^{TM} pad. The mfp, λ, is the average distance between interactions and is defined by eqn. 45, where λ_t is the average distance between any interaction. Diffusion theory was not chosen as it is most accurate when the thickness of a material is much greater than the mfp, where the thickness of Boral^{TM} is on the same order as the mfp across the entire energy range. A free-streaming approximation was applied to the He region as the neutron mfp in He is much greater than the thickness of He in the fuel cell.

$$\lambda_t = \Sigma_t^{-1} \tag{45}$$

The final step was to determine where the energy threshold should be set between the fast and thermal energy groups. This threshold determines which model was used for each energy group, ie. the thermal model was used for neutron energies below the threshold and the fast model was used for neutrons above the threshold. Figure 10 was used to determine where this threshold should be placed. This image shows the ratio $\frac{\Sigma_a}{\Sigma_t}$, where Σ_a is the absorption cross section. This graph shows the energy regions where absorption, the primary interaction in thermal energy regions, dominates the probability of reaction type. From figure 10, the energy threshold between the two models was set to 1 eV since below this region, absorption reactions

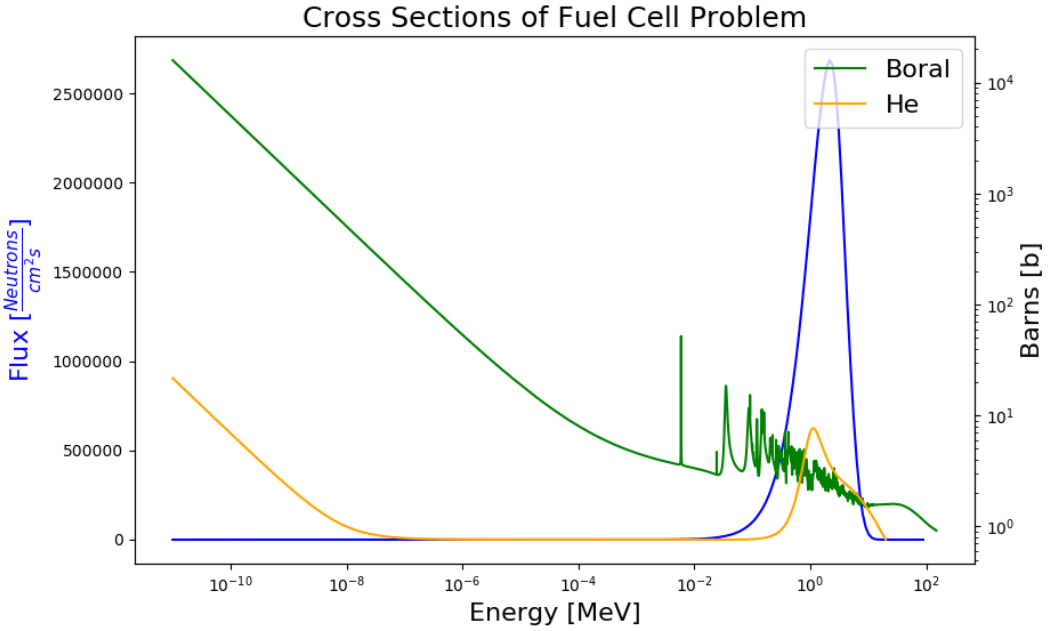

Figure 8: The cross section of materials present in the fuel cell region were plotted against the source spectrum to determine if a single group or multi-group model was needed to handle neutron transport.

are more probable even though the source flux is lower.

The final choice of an analytic model was a simplified version of the BTE. Here, we apply an isotropic scattering assumption which relaxes the directional dependence of Σ_s and assume isotropic flux which reduces the angular flux, φ, to the the scalar flux, ϕ. Eqns. 46 and 47, where the subscripts 1 and 2 refer to parameters in the fast group and thermal group respectively.

$$\hat{\mathbf{\Omega}} \cdot \nabla \phi_1 + \Sigma_{t,1}\phi_1 = \Sigma_{s,11}\phi_1 + S_1 \tag{46}$$

$$\hat{\mathbf{\Omega}} \cdot \nabla \phi_2 + \Sigma_{t,2}\phi_2 = \Sigma_{s,12}\phi_1 + \Sigma_{s,22}\phi_2 + S_2 \tag{47}$$

The integrals over energy, present in eqn. 5, in eqns. 46 and 47 are accounted for by averaging the cross section and flux terms across each energy region. The subscripts 1 and 2 (ie. $\Sigma_{t,1}$) denote the energy averaged cross section in the fast group, group 1, or the thermal group, group 2, respectively. Sec. 3.5 describes the calculations used to find these values.

The terms $\Sigma_{s,11}$ and $\Sigma_{s,22}$ are the in-group scattering terms for group 1 and group 2 respectively. The in-group scattering term accounts for scattering events that changes a neutron's energy, but does not remove the neutron from the group. Eqn. 47 depends on both $\Sigma_{s,12}$ and ϕ_1, as neutrons from group 1 will enter group 2 as a result of scattering interactions which decrease a neutron's energy below the lower threshold of group 1. Group 1 has no dependency on scattering interactions occurring in group 2, as we have assumed that a neutron in the thermal energy group will not gain enough energy from a scattering event to become a fast neutron again, a process called up-scattering. This is a fair assumption because there are no

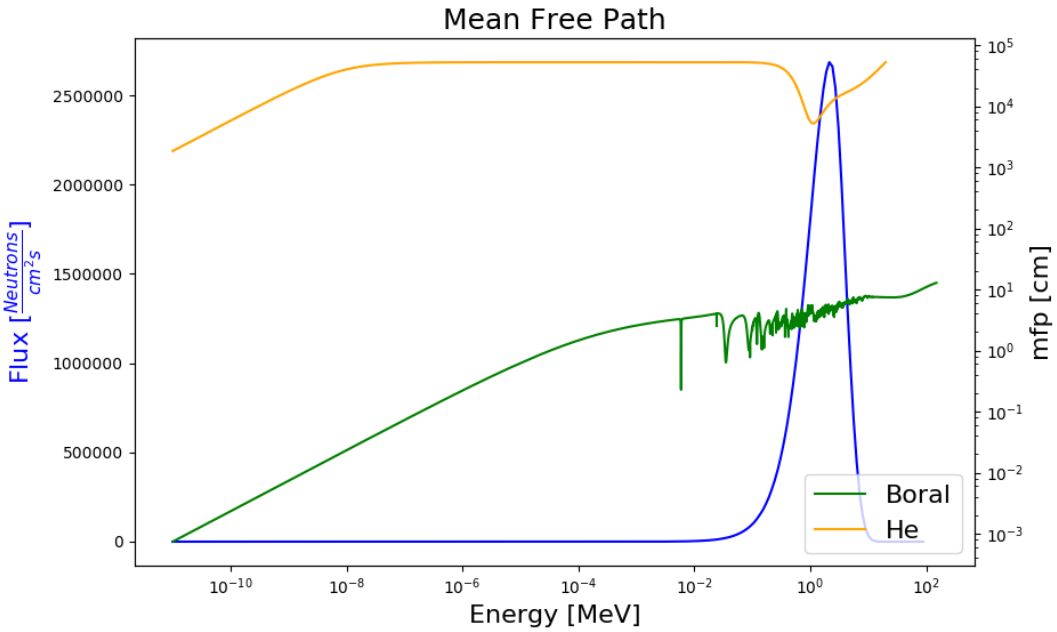

Figure 9: The mfp of materials in the fuel cell were plotted against the source spectrum. The source spectrum is present to qualitatively compare which energy regions are most important. Due to the large mfp of He, it was decided that the effect of neutron scatter events in He would contribute little to the transport problem from the fuel surface to the exiting boundary of Boral^{TM}. Therefore, neutrons in the He region were treated as free-streaming.

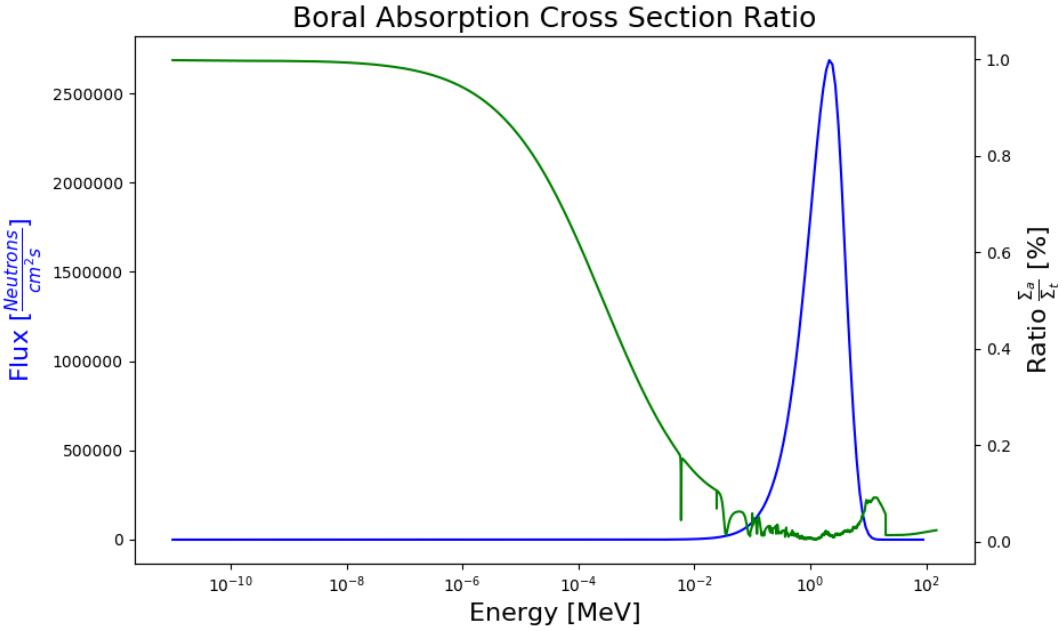

Figure 10: The ratio of $\frac{\Sigma_a}{\Sigma_t}$ was plotted to determine the energy cutoff between the fast and thermal neutron groups. The threshold was determined to be 1 eV since the absorption cross section begins to dominate below 1 eV.

atoms in the problem that are capable of imparting enough energy to a scattered neutron to increase the neutron's energy above 1 eV .

These equations are still difficult to solve after only considering a steady state assumption to eliminate time dependence. Therefore, more assumptions are applied to arrive at the final form of the two equations used in analytic calculations.

We first treat the sub-region as a 1-D planar geometry. This is a good assumption as the geometry of the fuel cell is symmetric in the x and y directions, allowing us to focus on the transport in either the x or y direction, the x-direction was chosen. The length of the problem in the z direction allows us to investigate the neutron transport along the x-axis independent of boundary effects from the the top and bottom of the fuel region, allowing us to remove z-dependence from our models. Variables that are defined by vectors (ie. $\hat{\mathbf{\Omega}}$) become 1-D scalars and the gradient operator reduced to its 1-D form, $\frac{\partial}{\partial x}$. Eqns. 48 and 49 are the result of the assumptions we have already applied. We have set our source s in both equations to zero, $S = 0$, since there are no neutrons being produced in Boral^{TM}.

$$\hat{\Omega}_x \frac{\partial \phi_1}{\partial x} + \Sigma_{t,1}\phi_1 = \Sigma_{s,11}\phi_1 \tag{48}$$

$$\hat{\Omega}_x \frac{\partial \phi_2}{\partial x} + \Sigma_{t,2}\phi_2 = \Sigma_{s,12}\phi_1 + \Sigma_{s,22}\phi_2 \tag{49}$$

The two equations are similar in form since our we have not made any assumptions about the physics that occurs in each individual region. We can make further assumptions by treating each energy group separately. We assume the fast region is scattering dominated resulting in the total cross section approximately being equal

to the scattering cross section, $\Sigma_t \approx \Sigma_s$. Rearranging the terms such that the fast group equation equals zero, leads to

$$\hat{\Omega}_x \frac{\partial \varphi_1}{\partial x} + (\Sigma_{s,1} - \Sigma_{s,11})\varphi_1 = 0. \tag{50}$$

Defining $\Sigma_{s,1}$ as

$$\Sigma_{s,1} \coloneqq \Sigma_{s,11} + \Sigma_{s,12}, \tag{51}$$

where $\Sigma_{s,12}$ is called the removal cross section of group 1 to group 2, $\Sigma_{R,12}$. Using definition 51 leads to the final form of the fast group BTE, eqn. 52, that will be used for analytic calculations in Boral^{TM}. The only mechanisms present in eqn. 52 are streaming and removal, principally due to scattering.

$$\hat{\Omega}_x \frac{\partial \varphi_1}{\partial x} + \Sigma_{R,12}\varphi_1 = 0. \tag{52}$$

Returning to eqn. 49, assume $\Sigma_{a,2} >> \Sigma_{s,22}$ and $\Sigma_{s,22} = 0$. We are assuming that scattering interactions only account for a small percentage of all interactions occurring in the thermal group. This assumption simplifies the group 2 total cross section to be approximately equal to the group 2 absorption cross section, $\Sigma_t \approx \Sigma_a$

The result of these two assumptions lead to the final form of the thermal group BTE used in analytic calculations, eqn. 53.

$$\hat{\Omega}_x \frac{\partial \varphi_2}{\partial x} + \Sigma_{a,2}\varphi_2 = \Sigma_{R,12}\varphi_1 \tag{53}$$

Note the dependence of eqn. 53 on φ_1. This is due to neutrons from the fuel primarily being born at fast energies, shown by the spent fuel spectrum, and no source of thermal neutrons being present in Boral^{TM}. Therefore, the only source of neutrons in the thermal group are those which down-scatter from the fast group.

3.5 Analytic Solution

After determining the simplified analytic models used for calculations, it is important to discuss how the cross section will be handled. Cross sections are energy dependent parameters that vary across the energy range of each group. Duderstadt and Hamilton describe a way to calculate average cross section values across an energy range [6]. Average cross section data is calculated by taking a flux weighted average across the energy range of interest, eqn. 54.

$$\langle \Sigma_x \rangle = \frac{\int_{E_{g-1}}^{E_g} \varphi_g \Sigma_x(E)}{\int_{E_{g-1}}^{E_g} \varphi_g} \tag{54}$$

g is the number of the group where $\langle \Sigma_x \rangle$ will be calculated across the energy range E_{g-1} to E_g, Σ_x corresponds to the cross section for reaction x, and φ_g is the flux in group g. Finding a solution to eqn. 54 is somewhat circular as the average cross section is needed to calculate the group flux and the group flux is needed to calculate the average cross section. Therefore, the source flux was used to determine the group flux in the fast and thermal groups. Once the flux through Boral^{TM} was found. This flux was used in eqn. 54 to check the initial averaged cross section values used in analytic models.

MCNP has a built in cross section plotter which calculates cross sections for materials based on atom percent of constituent isotopes which comprise that material.

The cross section plotter has an option to print an output table of of the cross section as a function of energy. Continuous energy cross section data was used in both MCNP calculations and to develop the tables used for calculating average cross section values used in the analytic models.

The removal cross section, $\Sigma_{R,12}$, was calculated using the following approximation provided by Lewis [5].

$$\Sigma_{R,12} \approx \frac{1}{n}\Sigma_s, \tag{55}$$

where n is the average number of collisions for a neutron to slow down from its original energy, E_0, into the thermal region, E. E_0 was taken to be approximately 1 MeV and E was 1 eV, the cutoff between the fast and thermal groups. In Boral^{TM}, n is approximately 125 collisions. In proposed work, a more rigorous method for calculating the removal cross section will be used based on solving a series of partial differential equations as outlined by Duderstadt and Hamilton [6].

The general solutions were found using mathematica to solve the ordinary differential equations for the fast and thermal regions. Eqns. 56 and 57 are the general solutions from eqns. 52 and 53 for the fast group and thermal group respectively.

$$\phi_1(x) = Ae^{-\frac{\Sigma_{R,12}x}{\mu}} \tag{56}$$

$$\phi_2(x) = \frac{A\Sigma_{R,12}e^{-\frac{\Sigma_{a,2}x}{\mu}+\frac{(\Sigma_{a,2}-\Sigma_{R,12})x}{\mu}}}{\Sigma_{a,2}-\Sigma_{R,12}} + Be^{-}\frac{\Sigma_{a,2}x}{\mu} \tag{57}$$

Eqns. 56 and 57 can be solved by applying the initial conditions, eqns. 58 and 59, respectively.In the initial conditions, ϕ_f are the values of the source flux corresponding to neutron energies above 1 eV, and ϕ_t are the values of the source flux corresponding to energies below 1 eV.

$$\phi_1(x=0) = \phi_f \tag{58}$$

$$\phi_2(x=0) = \phi_t \tag{59}$$

Using the initial conditions to determine values for A and B produces the final equations for the fast and thermal flux, eqns. 60 and 61 respectively.

$$\phi_1(x) = \phi_f e^{-\frac{\Sigma_{R,12}x}{\mu}} \tag{60}$$

$$\phi_2(x) = \frac{\phi_f\Sigma_{R,12}e^{-\frac{\Sigma_{a,2}x}{\mu}+\frac{(\Sigma_{a,2}-\Sigma_{R,12})x}{\mu}}}{\Sigma_{a,2}-\Sigma_{R,12}} + \frac{\phi_t(\Sigma_{a,2}-\Sigma_{R,12})-\phi_f\Sigma_{R,12}}{\Sigma_{a,2}-\Sigma R,12}(e^{-}\frac{\Sigma_{a,2}x}{\mu}) \tag{61}$$

A final adjustment was made to account for the presence of a source on the opposite side of the Boral^{TM} slab since a fuel cask contains a lattice of fuel bundles with Boral^{TM} pads being placed between two sources. A second source flux was geometrically attenuated from the location of the second source through the Boral^{TM} slab and added to the fast and thermal fluxes accordingly. The steel between the second source and Boral^{TM} Slab was assumed to negligibly alter the source flux. The final results of the fast and thermal fluxes are shown in figures 11 and 12.

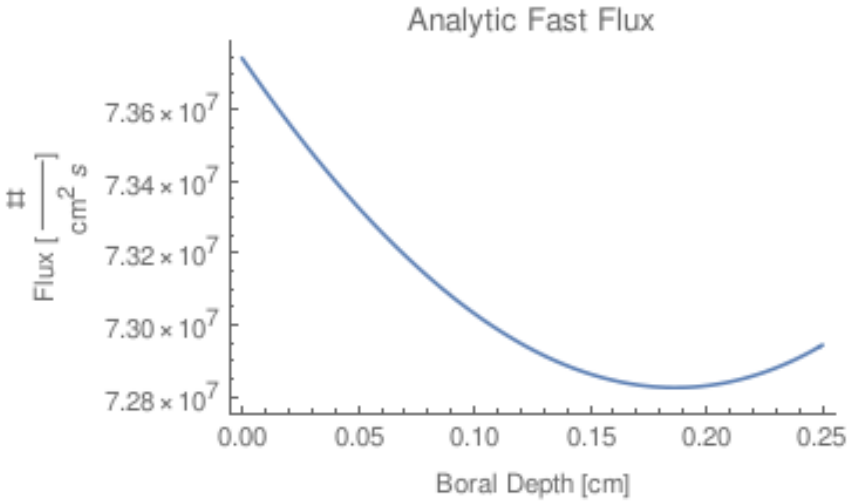

Figure 11: Analytic solution to eqn. 56

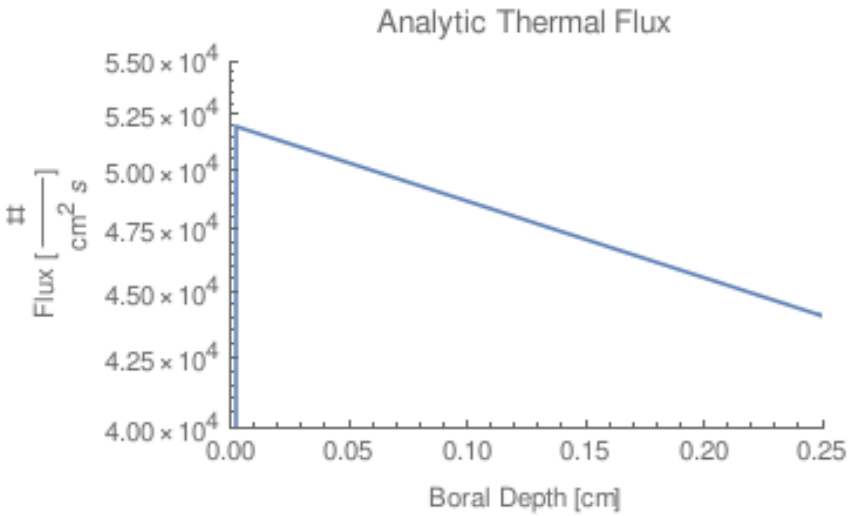

Figure 12: Analytic solution to eqn. 57

The analytic solution of the fast flux decays as a function of Boral^{TM} depth as a result of streaming and neutron scattering interactions removing neutrons from the fast group. This trend is expected as Boral^{TM} has no internal source to provide neutrons and the only mechanisms present in eqn. 52 are streaming and removal. However, there is an inflection point in the fast flux due to the second source as seen in fig. 11. The thermal flux has an initial value of $\approx 2\frac{neutrons}{cm^2 s}$. The thermal flux increases rapidly as fast neutrons down-scatter into the thermal group, shown in figfig:anaThermFlux. Absorption and streaming mechanisms cause the thermal flux to decrease as a function of penetration depth. The flux as a function of penetration into the Boral^{TM} pad will be compared to MCNP simulation results.

3.6 MCNP Simulation Results

The flux through the Boral^{TM} slab in a fuel cell was tallied using an FMESH tally across the entire Boral^{TM} slab. The mesh was designed to accommodate 50 cells across the thickness of the Boral^{TM} slab to acquire fine detail in the flux as a function of thickness. Figure 13 is the normalized flux as a function of depth through the Boral^{TM} slab.

The flux through the slab trends downward, as expected, before an inflection point, around 0.18 cm, shows the trend climbing. The upward trend at depths above 0.18 cm is a result of a second fuel bundle located on the opposite side of the Boral^{TM}.

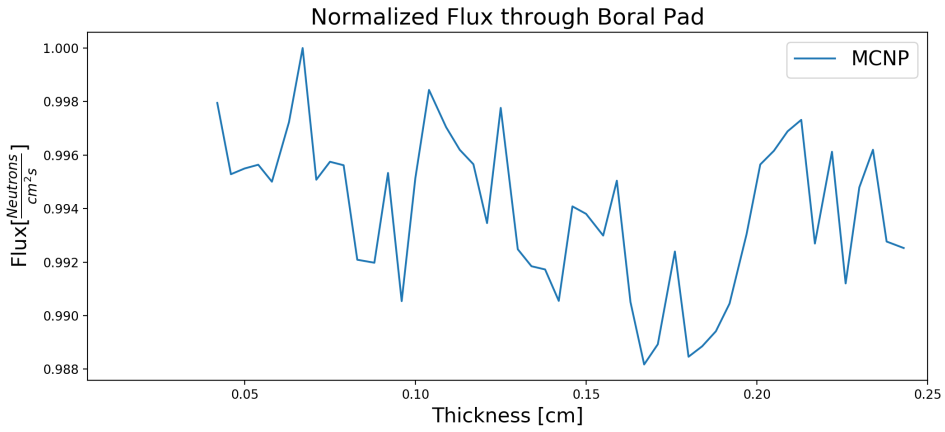

Figure 13: Results of the FMESH tally through the Boral^{TM} pad.

4 Comparison of Results

A comparison of the total flux determined through analytic methods and from MCNP simulations is provided in figure 14. The two fluxes agree well showing that the assumptions and approximations used to arrive at the analytic solution were credible.

From this process, we know the flux can be represented well using a two group model of the BTE, the interior layer of He can be neglected, the thermal flux is absorption dominated, the fast flux is scattering dominated, and the neutron

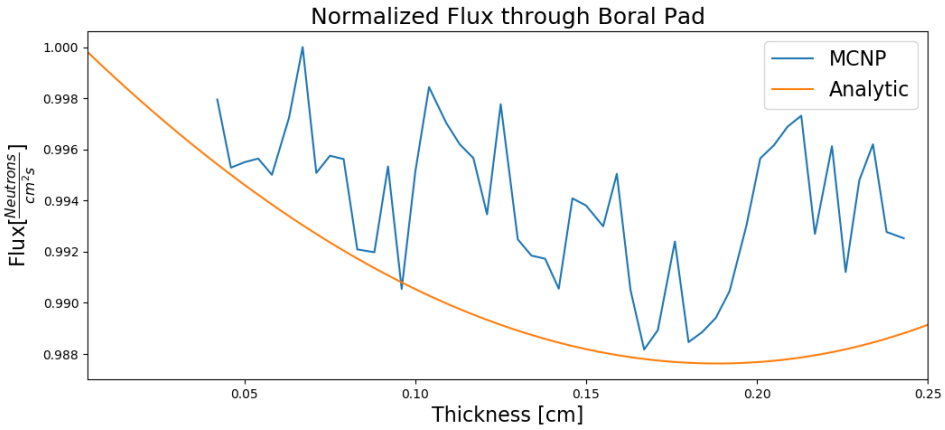

Figure 14: A comparison between the flux determined using analytic methods and MCNP simulations.

scattering can be treated as isotropic. While these are important conclusions, using the analytic solution to verify MCNP results can be more important to ensure the input file was correctly developed.

5 Future Work

In order to show this methodology leads to accurate and reliable analysis, it is important to identify other sub-regions in phase space where simplified theory can be applied. Five to six other sub-regions will be identified to show the versatility of this methodology. These sub-regions will likely not allow the same assumptions used in the fuel cell example.

While applying assumptions to the analytic models makes them tractable, solving more complex models reveals deeper physics governing the problem. Symmetry analysis will allow some assumptions to be relaxed while retaining a tractable model, yielding a more rigorous set of analytic models that those used in the fuel cell example.

Along with developing more complete analytic models, a more detailed HI-STORM 100 overpack and MPC model will be developed in MCNP. Gao showed that neutron transport in spent fuel casks is affected by geometry [19]. Therefore, a detailed MCNP model will be constructed where the geometry of the homogenized fuel region will be reduced to individual components and the air vents in the overpack will be changed to model the real-world air vents of the HI-STORM 100. Future sub-regions will be identified using the detailed MCNP geometry.

After comparing the results of the rigorous analytic models with the detailed MCNP simulations, a sensitivity analysis of the computational model will aid in identifying parameters that affect the calculated response from analytic models. The analytic models will then undergo a sensitivity analysis using the FSAP described by Cacuci. Finally, the results from the sensitivity analysis between computational and analytic models will be compared.

5.1 Timeline and Expected Papers

The timeline, table 5.1, describes the proposed time to completion of remaining tasks.

Task	Fall '18	Spr '19	Sum '19	Fall '19	Spr '20	Sum '20	Fall '20
Identification of sub-regions	X						
Development of detailed MCNP geometry	X						
Apply theory to sub-regions		X	X				
Comparison of results			X				
Id of input parameters for Sensitivity Analysis				X	X		
Find sensitivities of BTE using FSAP					X	X	
Write dissertation						X	X

We expect this work to be yield at least three papers. The first discussing the results of symmetry analysis on simplified forms of the BTE, a second paper on verifying nuclear simulations through comparison to analytic models, and the final paper describing the results of FSAP analysis of nuclear transport equations. This work is also suited for presentations in conferences such as those hosted by the American Nuclear Society and the Society of Physics Students-Division of Nuclear Physics.

6 Conclusion

The results of the fuel cell example provide evidence that analytic theory can be compared to MCNP simulations in order to gain a deeper understanding of the underlying physics in a problem and to verify the MCNP simulations were developed correctly. These results lend credence to the idea that confidence can be built in simulation result when experimental data is limited or non-existent by comparing computational solutions with analytic solutions. By identifying multiple, appropriate sub-regions in a problem, one is capable of developing a full understanding of the problem.

The purpose of this work is to gain a deeper understanding of the problem to better analyze the results of a simulation. The process of finding the analytic solution in the previous work reinforces the credibility of the assumptions used to develop our analytic models.

Simulation work has extended the complexity of problems which we can solve, making it an imperative tool for research. However, we can increase our knowledge of the underlying physics in a problem through analytic analysis which also be

used to verify simulation model accuracy. By identifying which sources of uncertainty have the most impact on a models response, we gain further knowledge of how a computational or analytic model can be improved to decrease the system's uncertainty.

References

[1] C. Greulich and et al., "High energy neutron transmission analysis of dry cask storage," *Nuclear Inst. and Methods in Physics Reserach, A*, vol. 874, pp. 5–11, 2017.

[2] C. J. Wharton, E. A. Seabury, A. J. Cafrey, and P. L. Winston, "Summary report: Inl cdcis cask scanner testing at doel, belgium," tech. rep., Idaho Natioal Lab, 2013.

[3] R. W. Jr., M. Fensina, and H. Trellue, "Total neutron emission generation and characterization for a next generation safegaurds initiative spent fuel library," *Progress in Nuclear Engineering*, vol. 80, pp. 45–73, 2015.

[4] "Hi-storm fsar," tech. rep., Holtec International.

[5] E. E. Lewis, *Fundamentals of Nuclear Reactor Physics.* Academic Press, 2008.

[6] J. J. Duderstadt and L. J. Hamilton, *Nuclear Reactor Analysis.* Wiley-Interscience, 1976.

[7] E. J. Alibright and et al., "Symmetry analysis of differential equations: A primer," Tech. Rep. LA-14502, Los Alamos National Lab, 2018.

[8] B. J. Cantwell, *Indroduction to Symmetry Analysis.* Cambridge, 2002.

[9] P. J. Olver, *Applications of Lie Groups to Differential Equations.* Springer, 1991.

[10] H. Wei and J. J. S. M. A. Nearing, "A comprehensive sensitivity analysis framework for model evaluation and improvement using a case study of the rangeland hydrology and erosion model," *Transactions of the ASABE*, vol. 50, no. 3, pp. 945–53, 2007.

[11] A. Saltelli and et. al., *Sensitivity Analysis in Practice.* John Wiley and Sons, New York, 2004.

[12] T. Turanyi and H. Rabitz, *Sensitivity Analysis.* Wiley, Inc., Chichester, 2000.

[13] D. G. Cacuci, *Sensitivity and Uncertainty Analysis: Theory.* Chapman and Hall/CRC, 2003.

[14] D. G. Cacuci, M. I. Ionescu-Bujor, and I. M. Navon, *Sensitivity and Uncertainty Analysis: Applications to Large-Scale Systems.* Chapman and Hall/CRC, 2005.

[15] W. F. G. van Rooijen and D. Lathouwers, "Sensitivity analysis for delayed neutron data," *Annals of Nuclear Engineering*, vol. 35, pp. 2186–2194, 2008.

[16] S. D. Ramsey, *The Extinction Probabilities of Nuclear Assemblies: A Sensitivity Study.* PhD thesis, University of Illinois at Urbana-Champaign, 2009.

[17] D. B. Pelowitz and et al., *MCNP6 User Manual.* Los Alamos National Lab, ver. 1 ed.

[18] J. K. Shultis and R. E. Faw, "An mcnp primer," tech. rep., Kansas State University, 2011.

[19] Y. Gao and et al., "Raditaion dose rate ditributions of spent fuel dry casks esitmated with mavric based on detailed geometry and continuous-energy models," *Annals of Nuclear Engineering*, vol. 117, pp. 84–97, 2018.

[20] A. Y. Chen and et al., "A comparison of dose rate calculations for a spent fuel storage cask by using mcnp and sas4," *Annals of Nuclear Engineering*, vol. 35, no. 2296-2305, 2008.

[21] "Scale: A comprehensive modeling and simulation suite for nuclear safety analysis and design," tech. rep., Oak Ridge National Lab, 2011.

[22] S. M. Bowman and I. C. Gauld, "Origin arp primer: How to perform isotopic depletion and decay calculations with scale/origen," tech. rep., Oak Ridge National Lab, 2010.